

Crystal Engineering in Continuous Plug-Flow Crystallizers

Maximilian O. Besenhard¹⁺, Peter Neugebauer²⁺, Otto Scheibelhofer¹, Johannes G. Khinast^{1,2*}

1 Research Center Pharmaceutical Engineering (RCPE), 8010 Graz, Austria

2 Graz University of Technology, Institute for Process and Particle Engineering, 8010 Graz, Austria

+) both authors contributed equally to this work

* Corresponding Author

Mail: khinast@tugraz.at Tel.: +43 316 873 30400 Fax: +43 316 873 1030400

Supplementary Information

1 Materials (additional information)

For assembly of the tubular crystallizer, straight and T-fittings consisting of PTFE with an inner diameter of 2.0 mm were used. Folded filters and round filters (Type MN 615, Macherey-Nagel, Germany) were used to separate the liquid from the crystalline phase. A sieving tower (AS200, Retsch, Germany) was used for isolating seed crystals (mesh sizes: 200 and 250 μm) from the commercial product.

The high-speed camera was an IDT NX-7-S2 (Imaging Solution GmbH, Germany) equipped with a 12X zoom lens system (Navitar, USA).

Microscope analysis was performed using a Leica DM 4000 microscope together with a Leica DFC 290 camera.

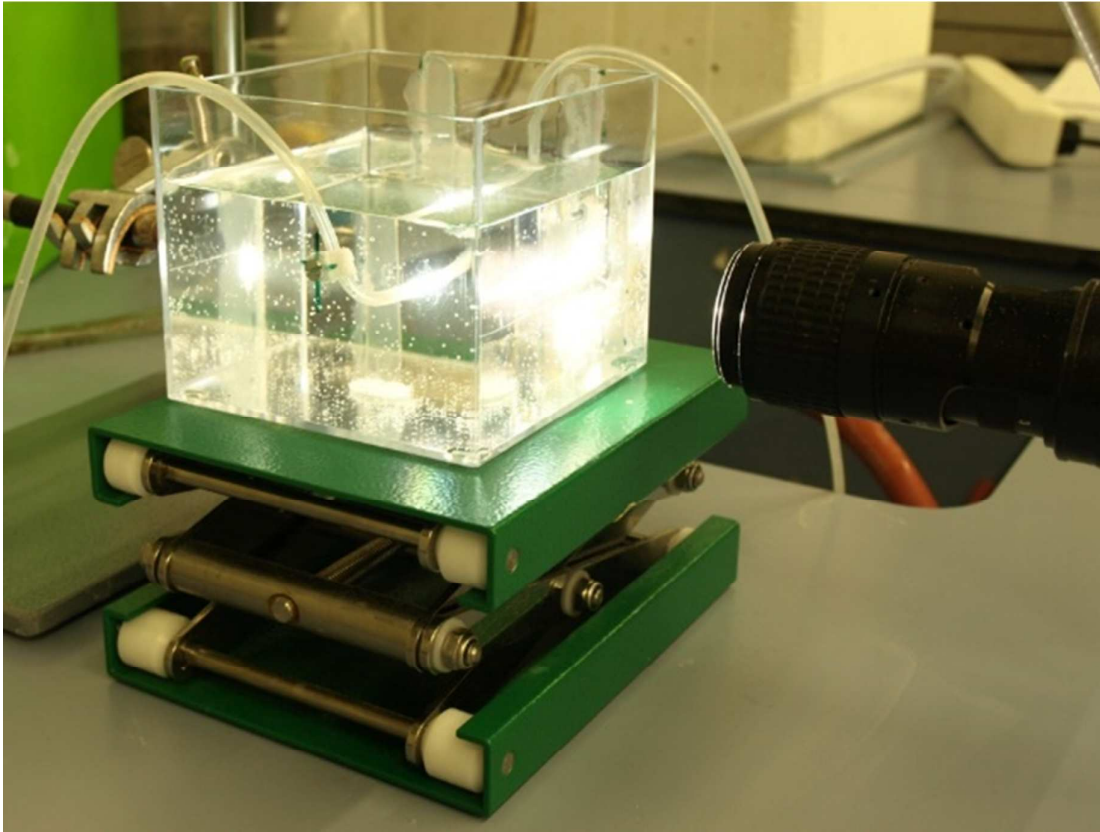
Raman spectroscopy was performed with a Perkin-Elmer Raman Station 400, Waltham, USA) and a Bruker Senterra Raman Microscope (Senterra II, Bruker, Karlsruhe, Germany).

FBRM measurements were performed using a FBRM field unit (Mettler Toledo, Leicester, UK).

2 Additional Information about Experiments and Results

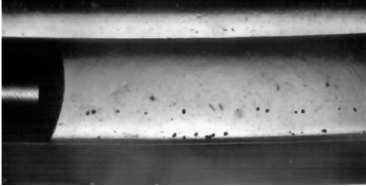
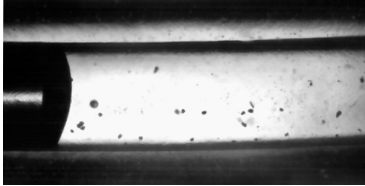

This section of the SI presents further details on the experimental set-ups, the data evaluation and material characterization, which are not provided in the main article.

2.1 Positioning of the High-Speed Camera



2.2 Particle Transport in a $d = 2$ mm Tubing

a)

Slow	Moderate	Fast
$\dot{V}_{tot} = \dot{V}_{Susp} + \dot{V}_{Air} = 8.7 \frac{ml}{min}$	$\dot{V}_{tot} = \dot{V}_{Susp} + \dot{V}_{Air} = 13.7 \frac{ml}{min}$	$\dot{V}_{tot} = \dot{V}_{Susp} + \dot{V}_{Air} = 18.7 \frac{ml}{min}$
$Ca \approx 0.64 \cdot 10^{-3}$	$Ca \approx 1.0 \cdot 10^{-3}$	$Ca \approx 1.4 \cdot 10^{-3}$
$m \approx 0.022$	$m \approx 0.028$	$m \approx 0.035$
$\delta_{film} \approx 19-25 \mu m$	$\delta_{film} \approx 26-32 \mu m$	$\delta_{film} \approx 32-37 \mu m$
		

b)

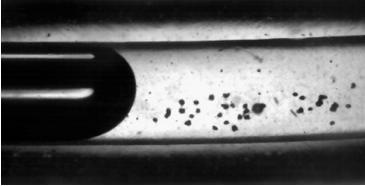
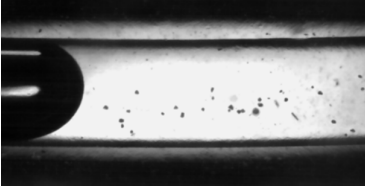
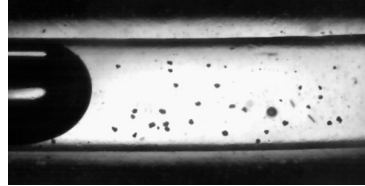
Slow	Moderate	Fast
$\dot{V}_{tot} = \dot{V}_{Susp} + \dot{V}_{Air} = 8.7 \frac{ml}{min}$	$\dot{V}_{tot} = \dot{V}_{Susp} + \dot{V}_{Air} = 13.7 \frac{ml}{min}$	$\dot{V}_{tot} = \dot{V}_{Susp} + \dot{V}_{Air} = 18.7 \frac{ml}{min}$
$Ca \approx 1.8 \cdot 10^{-3}$	$Ca \approx 2.9 \cdot 10^{-3}$	$Ca \approx 3.8 \cdot 10^{-3}$
$m \approx 0.042$	$m \approx 0.054$	$m \approx 0.063$
$\delta_{film} \approx 38-43 \mu m$	$\delta_{film} \approx 50-55 \mu m$	$\delta_{film} \approx 60-65 \mu m$
		

Figure S2: (a) Dispersion of small D-Mannitol particles (50-80 μm) in an air-liquid (saturated solution of mannitol in water) segmented flow. For all flow rates (slow, moderate & fast) $\dot{V}_{Susp}/\dot{V}_{Air} = 1.6$ no sedimentation, and hence the transport of crystals to subsequent segments was observed. (b) Dispersion of small D-Mannitol particles (50-80 μm) in a gas (air) liquid (saturated solution of mannitol in 40% water, 60% ethanol) segmented flow. For all flow rates (slow, moderate & fast) $\dot{V}_{Air}/\dot{V}_{Susp} = 1.6$. The latter ratio yielded shorter segments which is apparent from the videos. All videos are provided in the electronic SI.

2.3 Surface Tension Measurements of Pure and Saturated Solvent Mixtures

The surface tension was determined from contact angle measurement using the Easydrop (Krüss, Germany). All measurements were performed at room temperature (= 22°C).

Table S1: Surface tensions of pure and saturated ethanol-water solutions

Solution	Measurement 1 [$10^{-3} \cdot \text{N/m}$]	Measurement 2 [$10^{-3} \cdot \text{N/m}$]	Measurement 3 [$10^{-3} \cdot \text{N/m}$]	Measurement 4 [$10^{-3} \cdot \text{N/m}$]	Measurement 5 [$10^{-3} \cdot \text{N/m}$]	Average [$10^{-3} \cdot \text{N/m}$]
Water (deionized) ¹						~72
Ethanol 11%, water 89% (w/w) ¹						~46
Ethanol 50%, water 50% (w/w)	27.48	27.57	27.39	27.54	-	27.50 ± 0.08
Ethanol 50%, water 50% (w/w) saturated with (β) D-Mannitol	27.27	27.84	27.90	28.12	27.84	27.79 ± 0.32
Ethanol 60%, water 40% (w/w)	26.14	26.27	26.30	26.22	26.39	26.26 ± 0.09
Ethanol 60%, water 40% (w/w) saturated with (β) D-Mannitol	25.13	25.38	25.36	25.17	-	25.26 ± 0.13
Ethanol saturated with ASA	22.67	22.70	22.68	22.51	22.34	22.53 ± 0.18
Ethanol (99.8%)	21.73	21.83	21.74	21.69	21.81	21.76 ± 0.06

2.4 FBRM Measurements to Test Stability of D-Mannitol Crystal Size Distribution during Stirring

As described in the main article, the CSD of the starting suspension was, monitored for two hours during stirring via FBRM (FBRM field unit, Mettler Toledo, Leicester, UK). The results of these FBRM studies are shown in Figure S3.

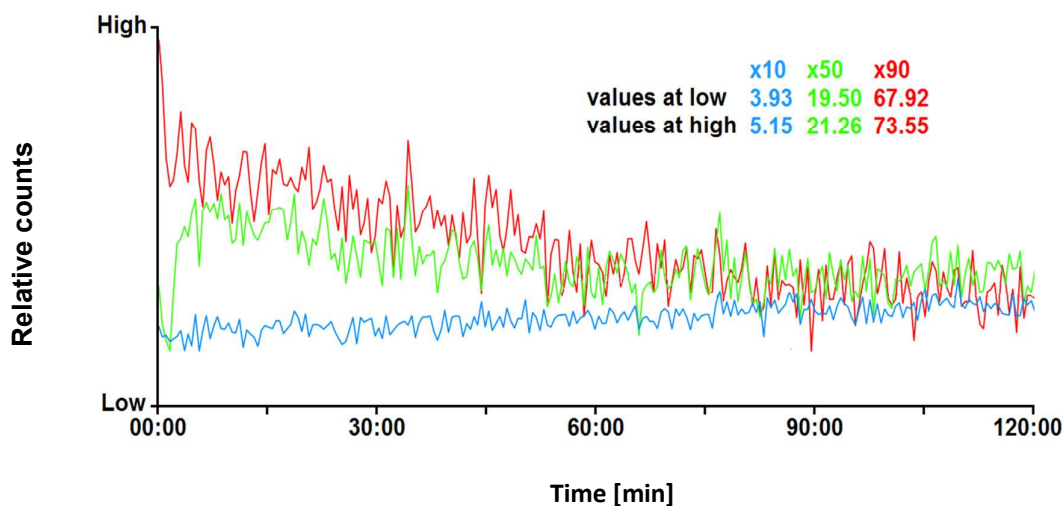


Figure S3: Results from the FBRM measurements, while stirring a D-mannitol suspension over 2h (mass fraction of solid D-mannitol in a saturated solution = 0.3 g/100g).

2.5 Stability of α -Polymorph in 60% Ethanol 40% Water (w/w) Solutions at 22°C

The stability of α -mannitol (non-commercial spray dried D-mannitol of high α -form content, Roquette, France) in a saturated solution of 60% ethanol and 40% water was investigated over a period of 60 minutes. A sieved fraction of α -mannitol (80 – 120 μm , mass fraction: 0.8 g/100 g solution) was suspended in 300 mL of the respective solution. The suspension was continuously stirred at 22°C using a magnetic stirrer. Samples of 20 ml were taken every 10 minutes, and filtrated while rinsing with acetone to eliminate water residuals. The Raman spectra of collected samples show no significant transition to the β -form, see Figure S.

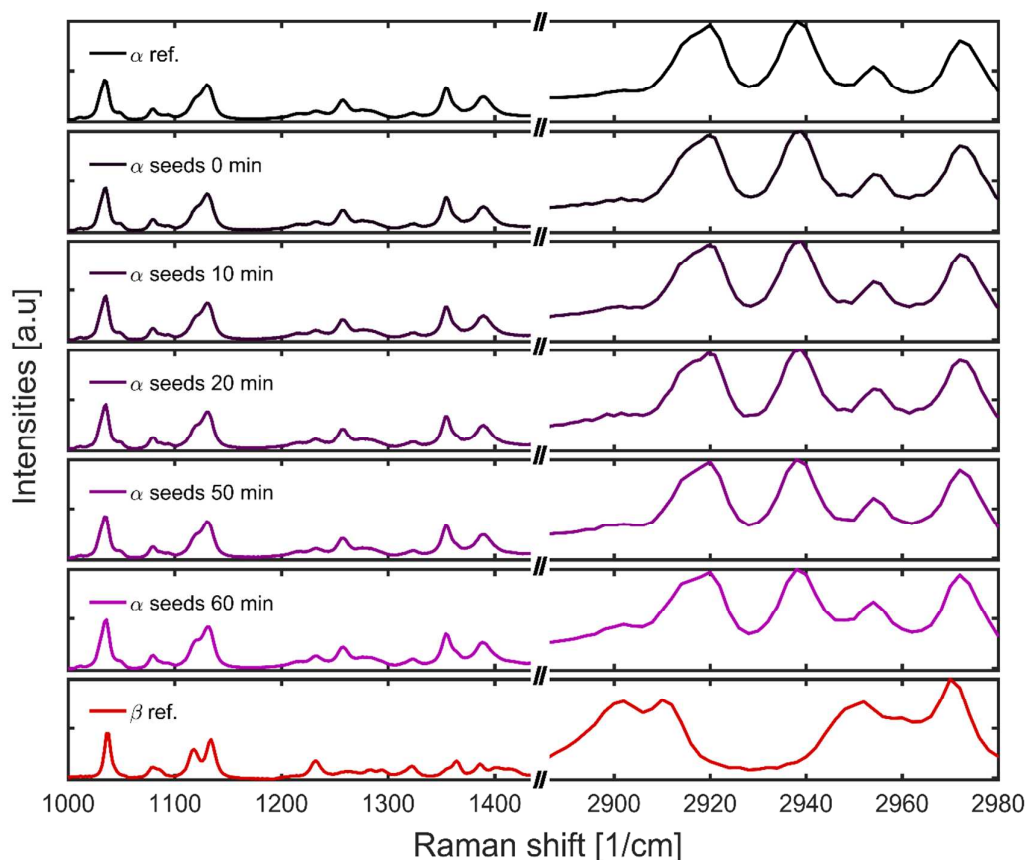


Figure S4: Raman spectra of the samples taken after 0, 10, 20, 50 & 60 min together with reference spectra of the α (non-commercial spray dried D-mannitol obtained from Roquette, France) and β (Pearlitol 160C, both from Roquette, France) form.

2.6 Raman Microscope Studies and Electron Micrographs

Seed particles and product crystals from experiments employing temperature cycling at $\Delta T = 20^\circ\text{C}$ and $\Delta T = 30^\circ\text{C}$ were examined using a scanning electron microscope (SEM) (Zeiss Ultra 55, Zeiss, Oberkochen, Germany) operated at 5 kV. The particles had been sputtered with gold-palladium prior to analysis. Results are shown in the main article, Figure 9 c-e.

3 Population balance equation model to model crystal size distribution during temperature cycling

This section of the SI presents the mathematical framework of the population balance model used to model the behavior of the crystal size distribution during temperature cycling. The results of this model are discussed in the article.

3.1 Temperature, concentrations and initial conditions

The temperature profile was modeled before solving the population balance equation (PBE), i.e., the energy and PBE are not coupled. Temperature changes due to enthalpy of crystallization have been neglected. The temperature profile was calculated as described formerly by our group². Used parameters are listed in Table S1

Table S2: Parameters used to calculate the Temperature profile.

Parameter	Value	Definition
d_{out}	0.004 [m]	outer diameter of the tubing
d_{in}	0.002 [m]	inner diameter of the tubing
α_{outer}	1000 [$\frac{W}{m^2 \cdot K}$]	outer heat transfer coefficient of the tubing
λ_{tubing}	0.3 [$\frac{W}{m \cdot K}$]	heat conductivity of the (silicone) tubing
$c_{p,slurry}$	2482 [$\frac{J}{kg \cdot K}$]	heat capacity of the slurry (~heat capacity of EtOH at 30°C)

The used population balance model assumes cubic crystals. Hence, the volume of a crystal is defined by

$$V_{cryst}(L) = k_v \cdot L^3 \quad (S1)$$

with a volume shape factor of $k_v = 1$.

The initial crystal size distributions (= normal distributions with $\mu = 180 \mu m$ and $\sigma = 180/2.5 \mu m$) are shown in Figure 5 of the main article. For all simulations, a solid mass ratio of 100 g/L was initialized. The solution was assumed to be saturated when starting the cycling procedure. For this model the solubility was adopted from the ASA solubility in ethanol using the Nývlt model presented by Maia.³

3.2 Population balance equation

As discussed formerly by our group² the population balance equation describing the temporal behavior of the crystal size distribution in a single segment (each segment is assumed to be

a single decoupled reactor) moving through the tube of length x_{tube} at a speed of $u_s = x_{\text{tube}}/t$ can be written as

$$\frac{\partial f(L, t)}{\partial t} + \frac{\partial (G(L, t) \cdot f(L, t))}{\partial L} = 0 \quad (\text{S2})$$

Here f denotes the number of particles with the internal coordinate L (i.e., the length of the cubic crystals, see Equation S1) at time $t = x_{\text{tube}}/u_s$. The used model solves equation S2 with f being number of particles per liter of suspension. G is the crystal growth rate which is positive in the case of growth and negative in the case of dissolution. Equation S1 does not account for changes in f due to aggregation and/or breakage or nucleation. If the growth rate is modelled to be size independent, Equation S1 can be simplified further by placing G in front of the brackets, i.e., not differentiate G with respect to L .

In the used model concentrations of the solute (c_{diss}), i.e., the dissolved molecules which are not in the crystalline phase, are presented in mol/L and changes were calculated via

$$\frac{\partial c_{\text{diss}}}{\partial t} = \frac{\partial c_{\text{diss}}}{\partial \left(\frac{x_{\text{tube}}}{u_{fs}} \right)} = - \frac{3}{M_w} \cdot k_v \cdot G \cdot q_c \cdot \int_0^\infty f(L, t) \cdot L^2 \cdot dL \quad (\text{S3})$$

with the molecular weight $M_w = 180$ g/mol and the density of the crystalline phase $\rho_c = 1400$ kg/m³.

The PBE was solved using the class-method (CM) by Kumar and Ramkrishna⁴ with more than 20,000 classes to discretize the crystal size distribution. The CM translates the partial differential equation S2 into a set of ordinary differential equations which was solved together with the mass balance equation S3 using Matlabs *ode45* solver.

3.3 Crystal growth

For positive growth rates, i.e., if the solution was supersaturated, a semi-empirical expression for G was used as in Lindenberg et al.⁵

$$G = k_{G1} \cdot e^{\left(-\frac{k_{G2}}{R \cdot T} \right)} \cdot c_{\text{diss}} \cdot \left(\frac{c_{\text{diss}}}{c^*} - 1 \right)^{k_{G3}} \quad (\text{S3})$$

In equation S3 c^* denotes the solubility of ASA, c_{diss} is the actual concentration of the solute, T the temperature (here in Kelvin) and R the gas constant in $J/(mol \cdot K)$. The used parameters are listed in Table S2. These parameters were chosen to have crystal growth of ~ 3 $\mu\text{m/s}$ if the supersaturation $S = c_{\text{diss}}/c^* = 1.5$.

Table S3: Growth rate parameters for crystal growth (Equation S3)

Parameter	Value
$k_{G1}=$	$22.47 \cdot 10^4 \left[\frac{\mu\text{m}}{\text{s}} \right]$
$k_{G2}=$	$2.58 \cdot 10^4 \left[\frac{\text{J}}{\text{mol}} \right]$
$k_{G3}=$	$1.00 [-]$

3.4 Crystal dissolution

For negative growth rates, i.e., if the solution was undersaturated, a semi-empirical expression for G was similar to Nagy et al.⁶

size independent dissolution rate

$$G = k_{D1} \cdot \left(\frac{Q_{sol}}{M_w} \cdot (c^* - c_{diss}) \right)^{k_{D2}} \cdot (1 + k_{D3})^{k_{D4}} \quad (S4)$$

size dependent

$$G(L) = k_{D1} \cdot \left(\frac{Q_{sol}}{M_w} \cdot (c^* - c_{diss}) \right)^{k_{D2}} \cdot (1 + k_{D3})^{k_{D4}} \cdot (1 + 1/e^{(1/100 \cdot L)}) \quad (S5)$$

The used parameters are listed in Table S4. These parameters were chosen to have crystal dissolution of $\sim 6 \mu\text{m/s}$ if the supersaturation $S = c_{diss}/c^* = 0.5$.

Table S4: Growth rate parameters for crystal growth (Equation S4)

Parameter	Value
$k_{D1}=$	$51.216 \left[\frac{\mu\text{m}}{\text{s}} \right]$
$k_{D2}=$	$0.9801 [-]$
$k_{D3}=$	$0.0202 [-]$
$k_{D4}=$	$0.8604 [-]$

3.5 Results not shown in the main article

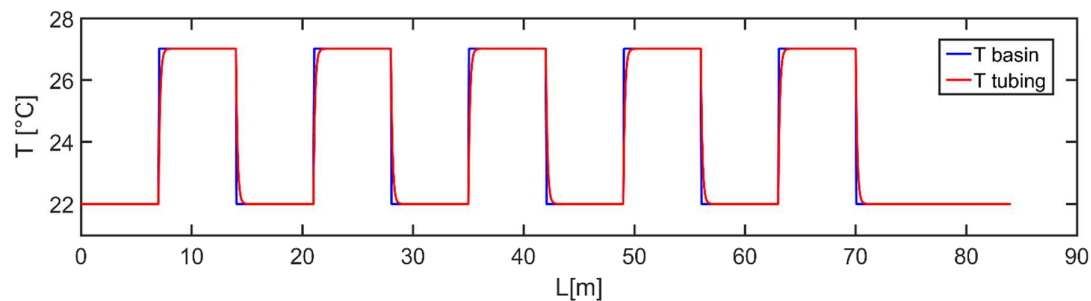


Figure S5: Temperature profile in the tubing, i.e. the segments, during temperature cycling.

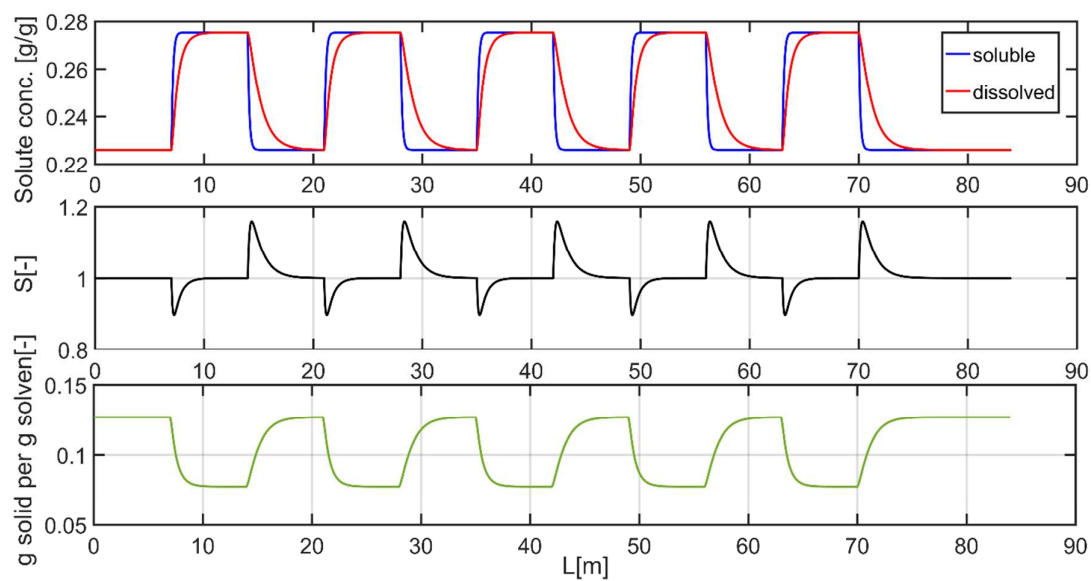


Figure S6: Concentration of dissolved species, supersaturation and amount of solid material during temperature cycling (size independent dissolution rate). The tube length (7.5 m in the heating and cooling basin) were chosen to allow equilibration ($S=1$) after every heating and cooling step.

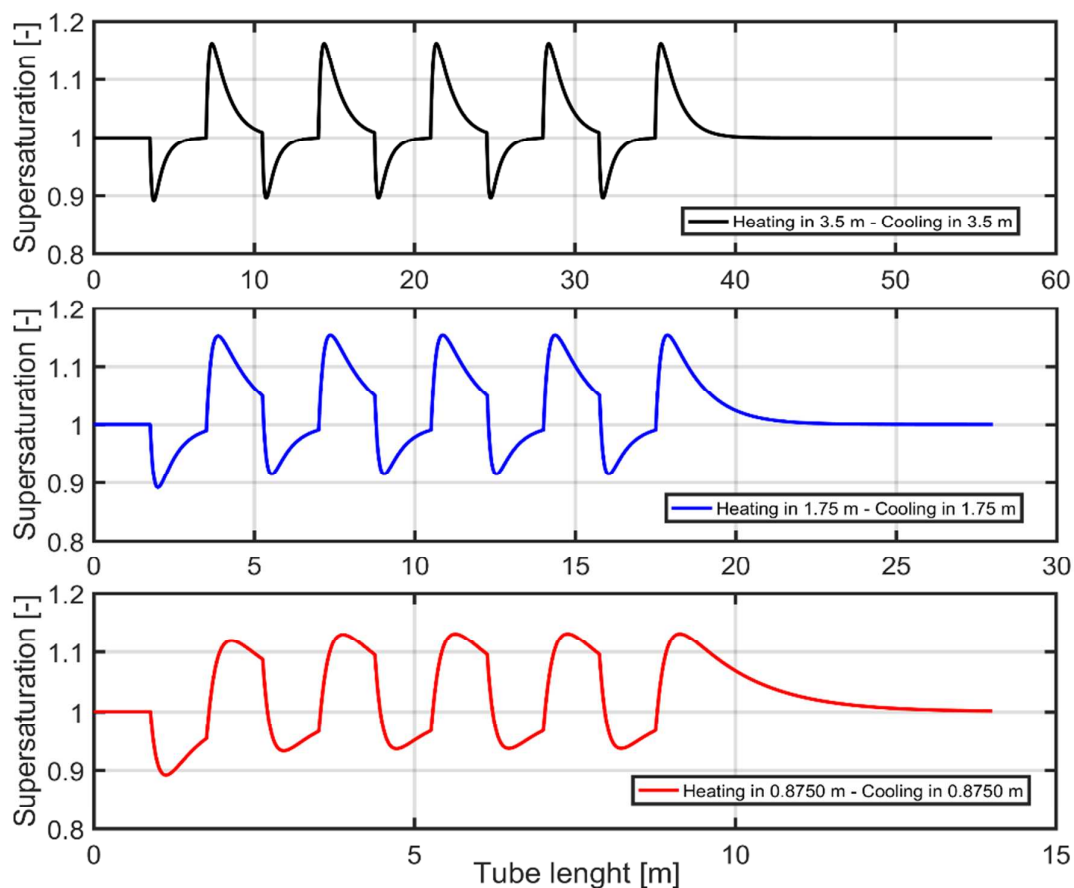


Figure S7: Supersaturation profiles during temperature cycling in different tube length but identical flow rates and temperature gradients (calculated using the size dependent dissolution model).

4 Quantification of α - and β -polymorph ratio via Raman spectroscopy and multivariate analysis

A multivariate approach, i.e., a PLS model, was chosen to quantify the fraction of the α -polymorph in a powder mixture consisting of the α - and β -polymorph via Raman spectroscopy. The part of the Raman spectra used for multivariate analysis is shown in Figure S.

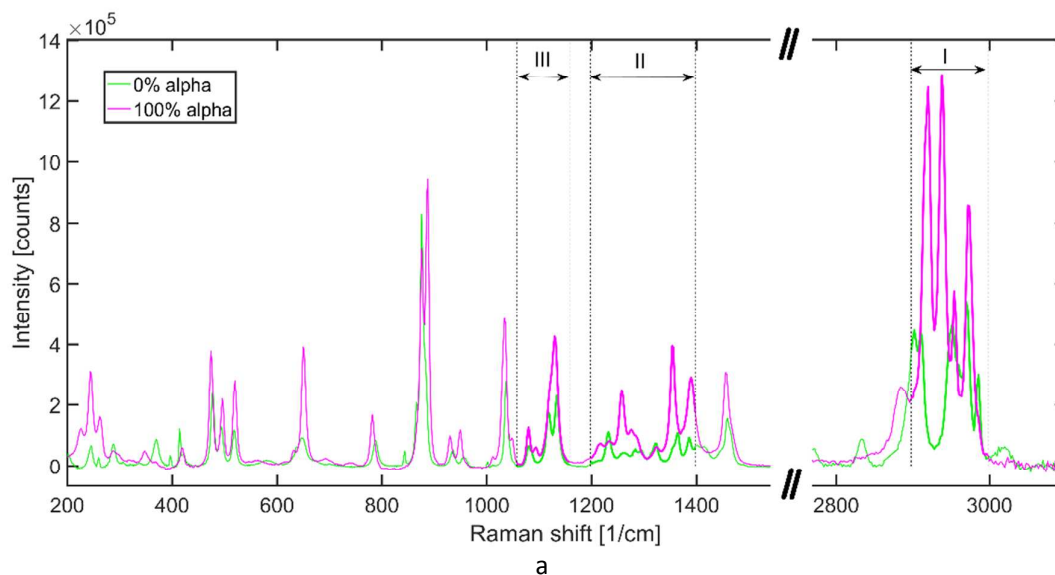


Figure S8: Raman spectra of α and β (= 0% α) polymorph (α -form: spray-dried type, non-commercial; β -form: Pearlitol 160C, both from Roquette, France, as received). The multivariate model used spectral data from regime I (2900-3000 cm^{-1}), II (1200-1400 cm^{-1}) and III (1060-1160 cm^{-1}) only.

To calibrate the PLS model 13 powder blends of a known α and β composition were prepared to record their Raman spectra. For each powder blend ten spectra were recorded at 100 different positions (= 1000 measurements per blend/sample) and then averaged. This was necessary to achieve consistent results, especially when the fraction of the α - or β -polymorph was low. Before performing the PLS, the spectral data of regime I-III have been merged (203 wavenumbers \rightarrow 203 data points) and normalized by equalizing the area under the merged spectra. The normalized intensities in the selected parts of the Raman spectra of the samples used for calibration are shown in Figure S9.

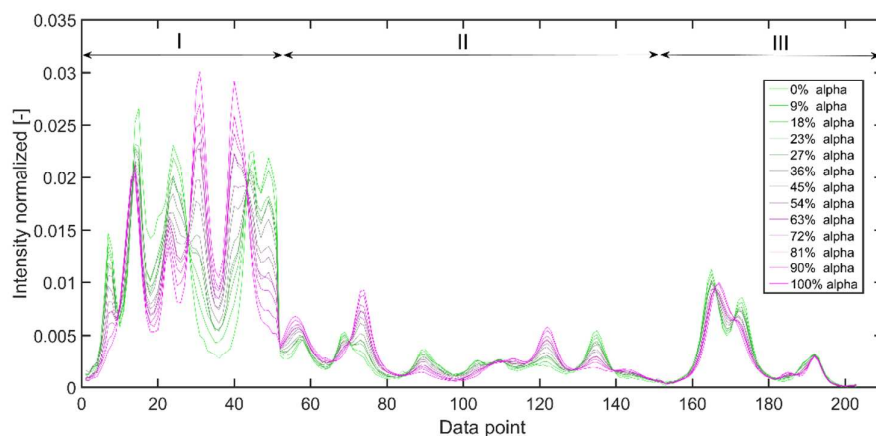


Figure S9: Normalized intensities of the selected parts of the Raman spectra. The arrows indicate the regime the data points originate from (same notation as in Figure S).

These normalized intensities of the 13 samples were united in the matrix X (13 rows, 203 columns) and the data of each column were mean-centered and scaled to unit variance. The PLS as defined in equation S6 was calculated using Matlabs® (R2016a, Mathworks, Natick, USA) statistic toolbox and the inbuilt function *plsregress*.

$$\begin{aligned} X &= \sum_{a=1}^A t_a \mathbf{p}_a^T + \mathbf{E} \\ Y &= \sum_{a=1}^A t_a \mathbf{q}_a^T + \mathbf{F} \end{aligned} \quad (\text{S6})$$

Y denotes the standardized (mean-centred and scaled to unit variance) observables, i.e., the fractions of the alpha polymorph. The exact fraction values are shown in Figure S10. a stands for the PLS dimension ($a = 1, 2, \dots, 12, 13$). \mathbf{p}_a , \mathbf{q}_a are the corresponding weighted loading vectors. \mathbf{E} and \mathbf{F} contain the remaining discrepancy between the PLS model and the data.

In order to avoid overfitting, the mean squared error of prediction using cross validation (*MSECV*) was determined as defined in equation S7. The *MSECV* quantifies the discrepancy between the predicted α fraction $\hat{Y}_{PLS i}$ (calculated by a PLS model generated from data of the 13 – 3 samples) and Y_i , i.e., α fraction in the 3 samples not used for model generation in the cross validation. This cross validation was performed 100 times, i.e., 100 models have been generated to evaluate 300 spectra.

$$MSECV = \frac{1}{100 \cdot 3} \cdot \sum_{i=1}^{100} \left\{ \sum_{k=1}^3 (\hat{Y}_{PLS i,k} - Y_{i,k})^2 \right\} \quad (\text{S7})$$

As expected the minimum *MSECV* of < 10 % α -fraction was achieved when using only the first latent variable ($a = 1$). This is because of the linear relation between Raman intensity and concentration. Since *MSECV* was in the range of 10% the error in the predicted α content is expected to be in the range of $\pm \sqrt{10}$ % (i.e., error < 4%). The model-prediction plot (using all 13 samples) is shown in Figure S10.

The Matlab files used for model development and spectra analysis are made available for download at the journals website.

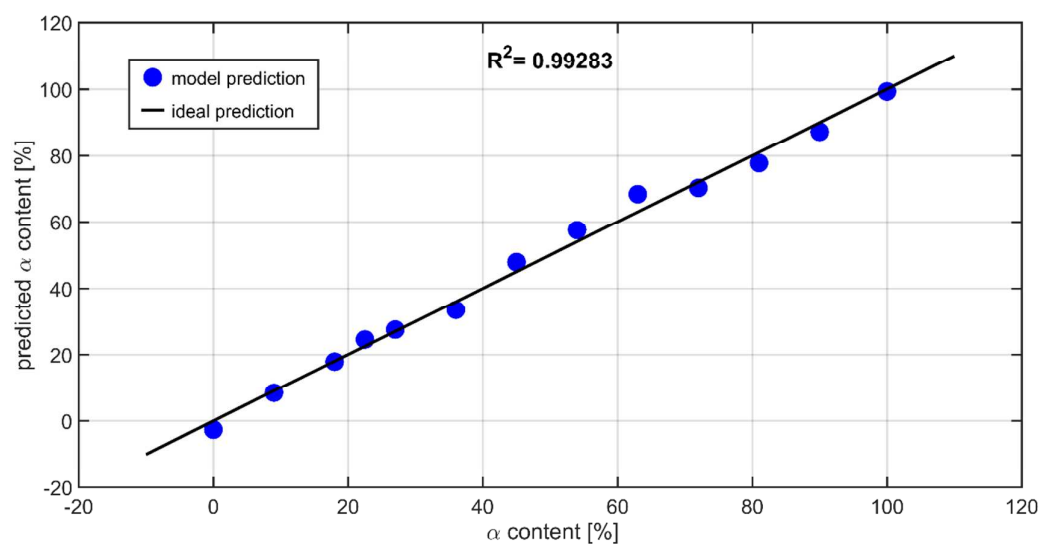


Figure S10: Model prediction of PLS model to quantify the α content. The ideal prediction is equivalent to the 1st median.

5 Determination of D-Mannitol solubility in water-ethanol solutions

The solubility of D-Mannitol (β -form) was obtained via density measurements as described by our group.² Solutions of known D-mannitol (β -form, Pearlitol 160C, Roquette, France, as received) concentrations in a 50:50 water-ethanol mixture and 40:60 water-ethanol mixture were prepared and their density was measured via the DM4500 (Anton Paar, Graz, Austria) densitometer. Solution preparation and density measurements were performed at 45°C, i.e., a temperature higher than the highest temperature of interest for the solubility measurements. The high precision densitometer allowed to correlate the density of the solution accurately with the D-Mannitol concentration, see Figure S12 & 13 (*top*). The solubility was measured by sampling the supernatant of a D-Mannitol (β -form) suspension that was stirred at the defined temperature for >2h through a filter. Density measurements of the withdrawn supernatants allowed to determine their concentration, see Figure S11 & S12 (*bottom*).

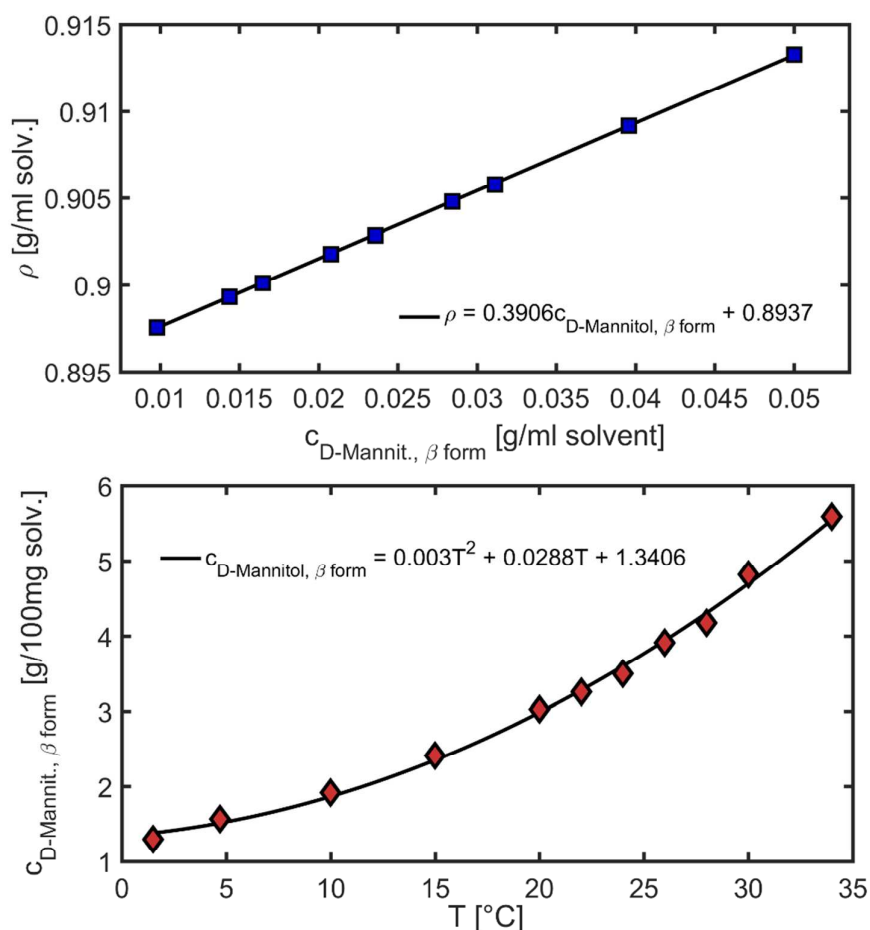


Figure S11: Solubility of D-Mannitol in a 50% water 50% ethanol (w/w). (*top*) Calibration curve, i.e., density of solutions with a known concentration measured at 45 °C. (*bottom*) Solubility curve obtained by measuring the density of the supernatant at 45 °C and the calibration curve (density of solvent = 0.8937 g/ml).

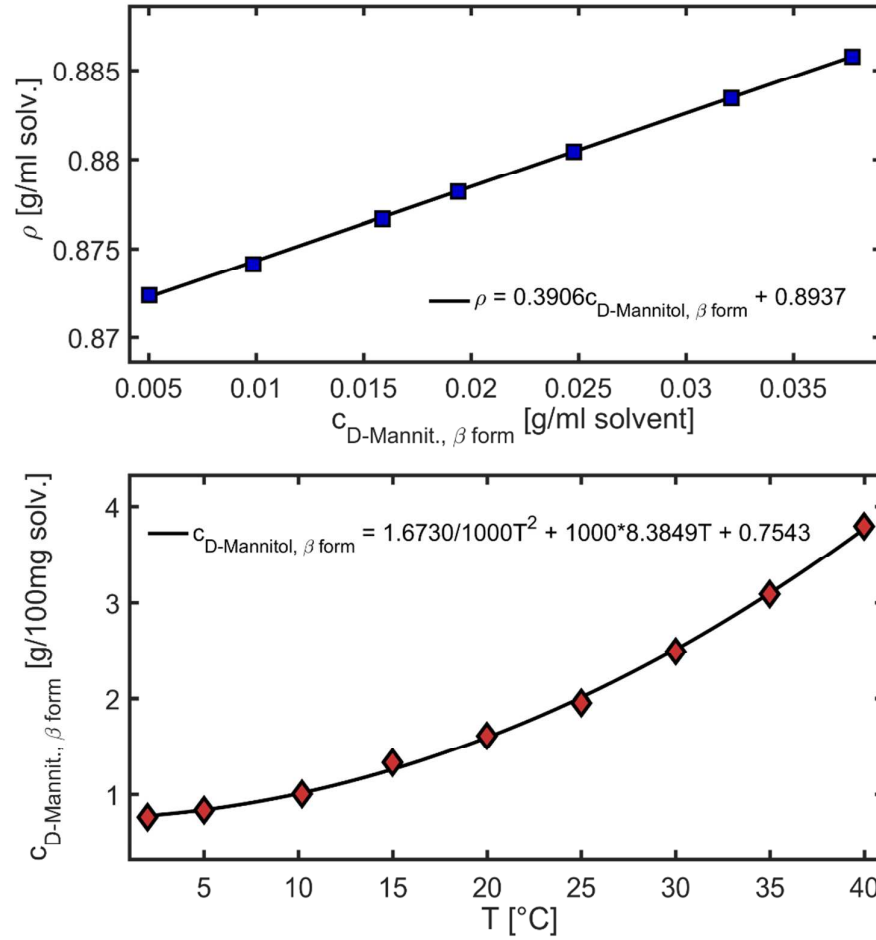


Figure S1: Solubility of D-Mannitol in a 40% water 60% ethanol (w/w). (top) Calibration curve, i.e., density of solutions with a known concentration measured at 45°C. (bottom) Solubility curve obtained by measuring the density of the supernatant at 45°C and the calibration curve (density of solvent = 0.8937 g/ml).

6 Estimation of Temperature Profiles

6.1 Estimation of Maximum Supersaturation during (3) Fines Trapping

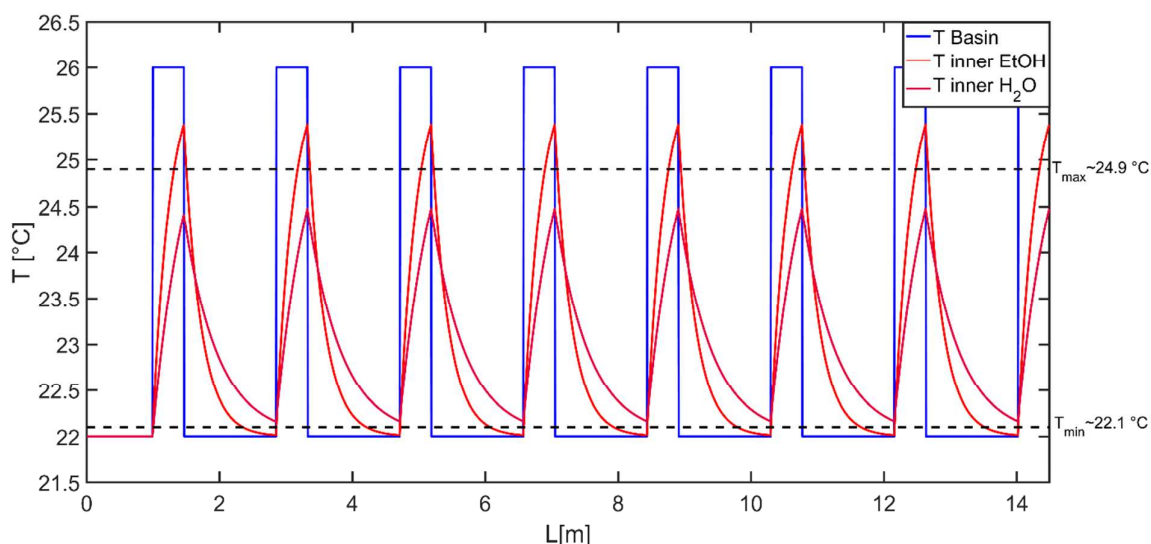


Figure S13: Estimated Temperature profile for pure water and ethanol in the tubing using the settings of the fine frapping studies (Delta T=6 °C).

Based on the temperature profile (calculated as described in section 3.1 of the SI and previously by our group²) and the process settings of the fine trapping studies (see section 3.2 of the article), as well as the heat capacities, densities, thermal conductivities and viscosities (the last three are used to calculate the Nusselt number/heat transfer coefficient) of pure water and ethanol, the maximum temperature was estimated as $T_{max} = 24.9^{\circ}\text{C}$ and $T_{min} = 22.1^{\circ}\text{C}$, (see Figure S13: Estimated Temperature profile for pure water and ethanol in the tubing using the settings of the fine frapping studies (Delta T=6 °C)). T_{max} was estimated as in the middle of the maximal temperature obtained during cycling of a pure ethanol and a pure water solution. The minimum temperature was estimated in the same way, but with a slight offset to the higher temperature. The latter is because the air gap (2 X 10 cm), i.e., the part of the tube that was not immersed in the water bed, was added to the 22°C batch although the heat transfer coefficient in air is lower (hence cooling is slower). Using the solubility for 50% water 50% ethanol (w/w) solutions shown in Figure S11: Solubility of D-Mannitol in a 50% water 50% ethanol (w/w). (top) Calibration curve, i.e., density of solutions with a known concentration measured at 45 °C. (bottom) Solubility curve obtained by measuring the density of the supernatant at 45 °C and the calibration curve (density of solvent = 0.8937 g/ml). these temperatures correspond to a maximum under saturations of $S_{min} = 0.85$ ($S_{22^{\circ}\text{C}} = 1$).

6.2 Estimation of Maximum Supersaturation during (5) Polymorphism Control

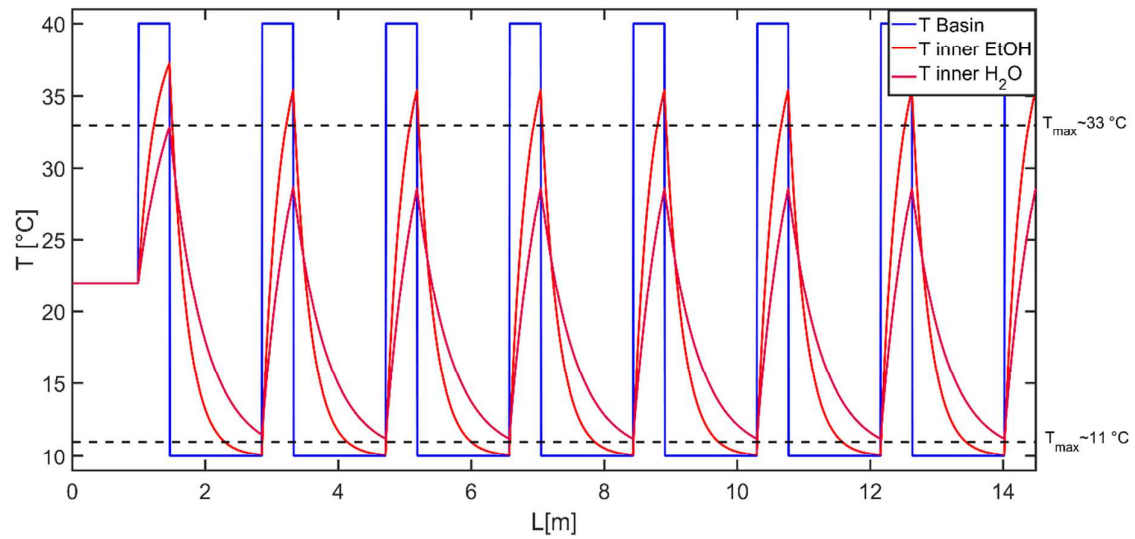


Figure S2: Estimated Temperature profile for pure water and ethanol in the tubing using the settings of the polymorphism control studies ($\Delta T=30\text{ }^{\circ}\text{C}$). Maximal and min

Using the same concept as in the previous section but the process settings of the polymorphism control studies (see section 5.2 of the article) the maximum temperature was estimated as $T_{min} = 11^{\circ}\text{C}$ and $T_{max} = 33^{\circ}\text{C}$, see Figure). Using the solubility for 40% water 60% ethanol (w/w) solutions shown in Figure these temperatures correspond to a maximum under saturations of $S_{min} = 0.7$ and $S_{max} = 1.9$ ($S_{22^{\circ}\text{C}} = 1$).

SI References

- (1) Speight, J. G. *Lange's Handbook of Chemistry*; 16th ed.; McGraw-Hill: New York, 2005.
- (2) Besenhard, M. O.; Hohl, R.; Hodzic, A.; Eder, R. J. P.; Khinast, J. G. Modeling a seeded continuous crystallizer for the production of active pharmaceutical ingredients. *Cryst. Res. Technol.* **2014**, *49*, 92–108.
- (3) Maia, G.; Giuliotti, M. Solubility of Acetylsalicylic Acid in Ethanol, Acetone, Propylene Glycol, and 2-Propanol. *J. Chem. Eng. Data* **2008**, *53*, 256–258.
- (4) Kumar, S.; Ramkrishna, D. On the solution of population balance equations by discretization—I. A fixed pivot technique. *Chem. Eng. Sci.* **1996**, *51*, 1311–1332.
- (5) Lindenberg, C.; Krättli, M.; Cornel, J.; Mazzotti, M.; Brozio, J. Design and Optimization of a Combined Cooling/Antisolvent Crystallization Process. *Cryst. Growth Des.* **2009**, *9*, 1124–1136.
- (6) Nagy, Z. K.; Aamir, E.; Rielly, C. D. Internal Fines Removal Using Population Balance Model Based Control of Crystal Size Distribution under Dissolution, Growth and Nucleation Mechanisms. *Cryst. Growth Des.* **2011**, *11*, 2205–2219.